Research Article

Timo Leppälä, Ahmed Gaber Abdelmagid, Hassan A. Qureshi, Konstantinos S. Daskalakis and Kimmo Luoma*

Linear optical properties of organic microcavity polaritons with non-Markovian quantum state diffusion

https://doi.org/10.1515/nanoph-2023-0749
Received October 29, 2023; accepted January 15, 2024;
published online February 9, 2024

Abstract: Hybridisation of the cavity modes and the excitons to polariton states together with the coupling to the vibrational modes determine the linear optical properties of organic semiconductors in microcavities. In this article we compute the refractive index for such system using the Holstein–Tavis–Cummings model and determine then the linear optical properties using the transfer matrix method. We first extract the parameters for the exciton in our model from fitting to experimentally measured absorption of a 2,7-bis[9,9-di(4-methylphenyl)-fluoren-2-yl]-9,9-di(4-methylphenyl) fluorene (TDAF) molecular thin film. Then we compute the reflectivity of such a thin film in a metal clad microcavity system by including the dispersive microcavity mode to the model. We compute susceptibility of the model systems evolving just a single state vector by using the non-Markovian quantum state diffusion. The computed location and height of the lower and upper polaritons agree with the experiment within the estimated errorbars for small angles ($\lesssim 30^\circ$). For larger angles the location of the polariton resonances are within the estimated error.

Keywords: microcavity polaritons; strong coupling; organic molecules

***Corresponding author: Kimmo Luoma**, Department of Physics and Astronomy, University of Turku, Turku, Finland, E-mail: ktluom@utu.fi. https://orcid.org/0000-0003-3118-612X
Timo Leppälä, Department of Physics and Astronomy, University of Turku, Turku, Finland, E-mail: tifile@utu.fi
Ahmed Gaber Abdelmagid, **Hassan A. Qureshi and Konstantinos S. Daskalakis**, Department of Mechanical and Materials Engineering, University of Turku, Turku, Finland, E-mail: ahmed.abdelmagid@utu.fi (A.G. Abdelmagid), hassan.qureshi@utu.fi (H.A. Qureshi), konstantinos.daskalakis@utu.fi (K.S. Daskalakis)

1 Introduction

The localized nature of molecular excitons imparts two crucial attributes: a large binding energy and a dense population of excitons compared to the photonic density of states. The former feature promotes strong light–matter coupling at room temperature, enabling the macroscopic study of Bose–Einstein condensation and superfluidity at elevated temperatures [1]–[4]. The latter feature enabled the observation of ultrastrong coupling [5] and single photon nonlinearity [6]. Recently, the concept of polariton chemistry was introduced, which promises to reshape the energy landscape of molecular systems, exerting control over their photochemical and photophysical processes [7]–[11]. In optical microcavities filled with molecular absorbers, polariton modes are the eigenstates resulting from the strong coupling between the optical modes and the exciton resonances. They can be observed experimentally as the avoided crossing of the bare exciton and microcavity photon dispersion through reflectivity measurements [12].

An interesting implication of strong coupling at nonzero temperature is that the exciton might also strongly couple to the surrounding molecular vibrations which can be the catalyst for complex relaxation dynamics of polaritons [13]. Currently, there is significant research being conducted to explore the impact of strong collective light–matter interactions on the intersystem crossing (ISC) and reverse intersystem crossing (RISC) rates [14]–[21]. Rabi splitting is proportional to the square root of the molecular density that share the microcavity photon ($\sqrt{N/V}$). To achieve strong coupling in planar microcavities with highly delocalized photonic mode, a large number of molecules N, in the order of 10^6 is needed. However, perturbative quantum mechanical calculations predict that possible polaritonic contributions to the RISC or ISC processes, for example, scale with inverse of this number [22]–[25].

The linear optical properties of organic microcavity polaritons have been investigated in the past using

various different methods. The coupling of the exciton to the vibrational modes can be modeled using the Holstein model (independent boson model) [26], [27] which can be exactly solved. When the molecules are placed into a microcavity the polariton dispersion relation can be observed in the collective strong coupling regime. A commonly used approach to extract the Rabi splitting is to fit the dispersion relation of coupled damped harmonic oscillators to the experimentally measured reflectivity spectrum [28], [29]. The coupling to the molecular vibrations can be included with more advanced approaches such as the input–output theory [30], [31], cumulant expansion [32]–[34], stochastic sampling of exact wave functions [35], Green's function methods [36], QM/MM simulations [22], few molecule models [37], and even single molecule models [38] to name a few.

The purpose of this article is to introduce a new method for investigating the polariton dynamics and pave the way for gaining new insights into the so called "large number of molecules N" problem. In this work we take the first steps of applying non-Markovian quantum state diffusion (NMQSD) for computing the linear optical properties of organic microavity polaritons. While a possible drawback of this approach is that it is stochastic and typically requires a large number of trajectories for computing expectation values of observables, for computing linear optical properties using just one trajectory is enough [39]–[41]. In contrast to computing the response of polaritons from the response of the cavity modes alone, as in [38], [42] for example, we use NMQSD to compute the linear response of the combined exciton cavity mode system which is probed by classical electromagnetic field. This means that we consider a situation where the light that is transmitted through the cavity mirrors may be directly absorbed by both the cavity modes and the molecules. Excluding the molecular absorption results in high absorption of the upper polariton at higher angles of the incoming light, which is in conflict with experimental data. From the response function (linear susceptibility) we obtain the index of refraction which is used then in solving the Maxwell equations corresponding to the experimental setup.

We present a graphical summary of this article in Figure 1. (a) We use the transfer matrix method (TMM) to compute the reflectivity, transmission, and absorption of the system when it is probed by a classical electromagnetic field. We assume that the response of the system is linear. Then the macroscopic properties of the sample are determined by the index of refraction which is obtained from the linear susceptibility $\chi(\omega)$. We use NMQSD to compute this in the model systems evolving just a single state vector. (b) The susceptibility of a thin film is modeled by the susceptibility of just one molecule multiplied by the dipole number density. We fit a model to the experimental data and extract the values for the parameters of the organic semiconductor exciton. (c) The microcavity system is modeled by a slab of molecules interacting with a microcavity mode. The susceptibility is computed by evolving now a single pure state of a system of N molecules interacting with K cavity modes using NMQSD.

The structure of this article is the following. In Section 2 we introduce the linear response theory and how the susceptibility and refractive index can be computed. In Section 3 we introduce the NMQSD method. Furthermore, we show how the susceptibility can be computed using the NMQSD approach. Then in Section 4 we fit the model

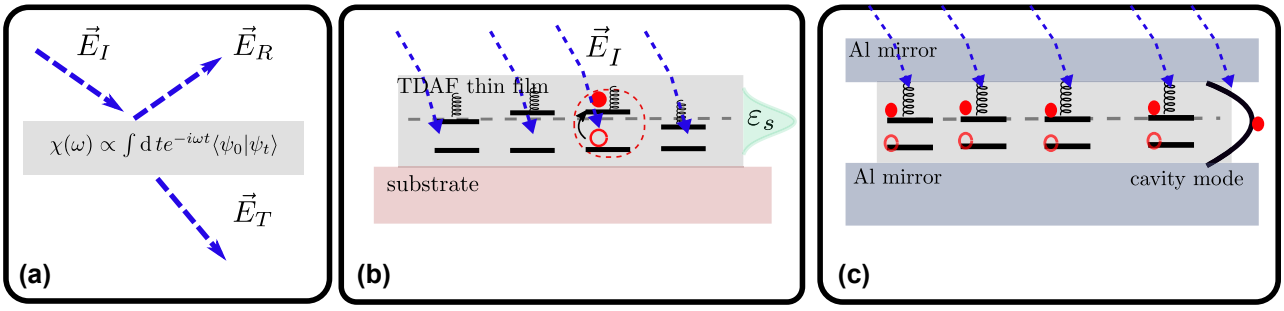

Figure 1: Measurement and systems considered in this article. (a) We model the linear optical properties of a slab of material in terms of the dielectric function ε, which can be computed from the susceptibility χ. The susceptibility is computed from a quantum mechanical model evolving just a single state vector. This leads to a computationally efficient scheme in contrast to approaches where density matrix evolution is needed. In the other panels we describe which kind of system we consider. (b) Susceptibility of a thin film can be modeled as the susceptibility of a single quantum absorber (red circle) multiplied with the number of such absorbers, when spatial disorder can be neglected. We include energetic disorder as indicated by the distribution of exciton energies ε_s, and a coupling to vibration modes when the system is excited (indicated by the spring). As the molecule absorbs a photon an exciton is formed indicated by the red filled and empty circles. (c) In the case of microcavity polaritons we consider a slice of emitters in the z-direction, whereas the cavity mirrors are located at $x = \pm L/2$ (top and bottom). The cavity mode is represented by the parabolic curve between the mirrors. The incoming light may be absorbed *coherently* by the molecules and the cavity mode, which is indicated by the *superposition* of excitons in the molecule and an excitation in the cavity mode.

parameters to the single molecule data obtained from experimental measurements and density functional calculations. We will focus on 2,7-bis[9,9-di(4-methylphenyl)-fluoren-2-yl]-9,9-di(4-methylphenyl) fluorene (TDAF) as it is a model system for strong light–matter studies [21], [43], [44]. In Section 5 we construct the model for microcavity polaritons using the same TDAF molecule. We discuss in detail how the susceptibility can be computed in this case when the dispersive microcavity mode is also included. We also present the results of the theoretical calculations. In Section 6 we present our conclusions and outlook. Experimental details are presented in Section 7.

2 Linear response

2.1 Linear optics

In linear materials the polarization field is proportional to the applied electric field

$$\mathbf{P}(t,z) = \int_0^t \mathrm{d}s \int \mathrm{d}z'\, \varepsilon_0 \chi(t-s, z-z')\mathcal{E}(s,z'), \tag{1}$$

where ε_0 is the vacuum permittivity and χ is the susceptibility. We set $\hbar = 1$ in all subsequent equations. Due to causality polarization can depend only on the fields applied on earlier times and may have non-local spatial dependency [45]. In general, χ is a second rank tensor. In this work we focus only on situations where the polarization is aligned with the applied electric field making χ a scalar. By using the convolution theorem and after dropping the vector notation this relation is

$$P(\omega, k_z) = \varepsilon_0 \chi(\omega, k_z)\mathcal{E}(\omega, k_z), \tag{2}$$

where ω is the angular frequency and k_z is the z-component of the wave vector. The dielectric function (or relative permittivity) is

$$\varepsilon(\omega, k_z) = 1 + \chi(\omega, k_z). \tag{3}$$

The dielectric function determines the refractive index by $n = \sqrt{\varepsilon}$. Once the refractive index is known, the linear optical properties of planar systems can be computed using the transfer matrix method (TMM) [46].

2.2 Dipole density

Polarization corresponds to the dipole density of the medium, which can be computed from a microscopical model. We consider a situation where weak field is used to probe a quantum system. The interaction term between the classical electromagnetic field and the matter is taken to be

$$H_F(t) = -\sum_m \mathcal{E}(z_m, t) \cdot \mu_m, \tag{4}$$

where z_m is the location of a point dipole and μ_m is the dipole operator. The other degrees of freedom are described by a time independent Hamilton operator H. The dynamics generated by H is given by the unitary operator

$$U(t) = \mathrm{e}^{-\mathrm{i}Ht}. \tag{5}$$

The linear response can be computed from the dipole correlation function $M(t)$ [39], [40], [47]. The susceptibility of the system can be computed as the Fourier transform of $M(t)$

$$\chi(\omega, k) = \int_0^\infty \mathrm{d}t\, \mathrm{e}^{\mathrm{i}\omega t} M(t, k_z), \tag{6}$$

where

$$M(t, k_z) = \sum_{m,n} e^{ik_z(z_m - z_n)} \langle \Psi_G | \mu_n U(t) \mu_m | \Psi_G \rangle, \tag{7}$$

and $|\Psi_G\rangle$ is the ground state of the Hamiltonian H. We assume that the systems we investigate do not have permanent dipole moment. Under this assumption the dipole correlation function is obtained from perturbation theory and keeping only the positive energy terms and the terms linearly proportional to the applied field [48], [49]. Generalization to anisotropic cases is straightforward. Using Eqs. (2) and (6) gives the polarization density of the system. The macroscopic polarization is obtained by multiplying the polarization density with the sample volume. In this work we neglect any spatial disorder. Finite temperature results can be computed using the ground state initial condition in the NMQSD approach as we show later. Alternative methods for solving Eq. (7) exist such as cumulant expansion techniques [33], [34] or exact stochastic wave function sampling [35].

3 Non-Markovian Quantum State Diffusion

3.1 General theory

The aim of the NMQSD approach is to solve the time evolution of the full Schrödinger equation for the open system and the environment [50]–[52]. A typical model consists

of an open system with Hamiltonian H_S and a coupling operator L. These operators are arbitrary at this point. The environment is assumed to consist of quantum harmonic oscillators with a Hamiltonian

$$H_E = \sum_\lambda \omega_\lambda b_\lambda^\dagger b_\lambda, \tag{8}$$

where $\left[b_\lambda, b_{\lambda'}^\dagger\right] = \delta_{\lambda,\lambda'}$. Generalization to spin baths is possible [53]. The interaction is taken to be linear in the coupling operator L of the open system and the creation and annihilation operators of the environment

$$H_I = \sum_\lambda g_\lambda L b_\lambda^\dagger + g_\lambda^* L^\dagger b_\lambda. \tag{9}$$

The initial state of the bath is the thermal state ρ_β and the system and the bath are initially uncorrelated. In the interaction picture with respect to (8) the Schrödinger equation is

$$\frac{\mathrm{d}}{\mathrm{d}t}|\Psi_t\rangle = -iH_S|\Psi_t\rangle + \sum_\lambda \left(g_\lambda L b_\lambda^\dagger \mathrm{e}^{\mathrm{i}\omega_\lambda t} + h.c.\right)|\Psi_t\rangle \tag{10}$$

The finite temperature NMQSD equation corresponding to the Schrödinger equation (10) is [50]

$$\frac{\mathrm{d}}{\mathrm{d}t}|\psi_t(\mathbf{z}^*)\rangle = -i(H_S + V(t))|\psi_t(\mathbf{z}^*)\rangle + z_t^* L|\psi_t(\mathbf{z}^*)\rangle - L\int_0^t \mathrm{d}s\, \alpha(t-s)\frac{\delta}{\delta z_s^*}|\psi_t(\mathbf{z}^*)\rangle, \tag{11}$$

where z_t^* is a zero mean Gaussian stochastic process with correlations

$$\mathcal{M}\left[z_t z_s^*\right] = \alpha(t-s), \quad \mathcal{M}\left[z_t z_s\right] = 0. \tag{12}$$

The Hermitian autocorrelation of the process corresponds to the zero temperature bath correlation function (BCF)

$$\alpha(t-s) = \int_0^\infty \mathrm{d}\omega\, J(\omega)\mathrm{e}^{-\mathrm{i}\omega(t-s)}, \tag{13}$$

We have introduced the spectral density $J(\omega) = \sum_\lambda |g_\lambda|^2 \delta(\omega_\lambda - \omega)$, which controls the properties of the environment.

Finite temperature is incorporated by a "stochastic potential" $V(t)$

$$V(t) = L\eta_t + L^\dagger \eta_t^*, \tag{14}$$

where η_t is a zero mean Gaussian stochastic process with correlations [51], [54]

$$\mathcal{M}\left[\eta_t \eta_s^*\right] = \sum_\lambda n_\lambda |g_\lambda|^2 \mathrm{e}^{-\mathrm{i}\omega_\lambda(t-s)}, \tag{15}$$

and $n_\lambda = \left(\mathrm{e}^{\beta\omega_\lambda} - 1\right)^{-1}$ is the thermal photon number. The NMQSD equation is a stochastic differential equation containing the Hamiltonian term, stochastic driving term and a memory term with a functional integral. The open system states $|\psi_t(\mathbf{z}^*)\rangle = \langle \mathbf{z}\|\Psi_t\rangle$ are analytical functionals of the noise process $z_t^* = -i\sum_\lambda g_\lambda z_\lambda^* \mathrm{e}^{-\mathrm{i}\omega t}$, where z_λ^* are the labels of the Bargmann coherent states $||\mathbf{z}\rangle = \prod_\lambda e^{z_\lambda a_\lambda^\dagger}|0\rangle$ of the environment [52]. By construction the exact open system is recovered by averaging over the stochastic trajectories

$$\rho(t) = \mathrm{tr}_E\{|\Psi_t\rangle\langle\Psi_t|\} = \mathcal{M}\left[|\psi_t(\mathbf{z}^*)\rangle\langle\psi_t(\mathbf{z}^*)|\right]. \tag{16}$$

The NMQSD approach works in general with an arbitrary bath correlation function. For example, bath correlation functions obtained from surrogate harmonic bath embeddings such as in Ref. [38] could be incorporated into our formalism. The challenging part in using NMQSD is the occurrence of the functional derivative. In recent years a powerful hierarchy of pure states (HOPS) approach has emerged as a general numerical approach to solve the NMQSD equations [51], [55]. We explain next the weak coupling approximation for the functional derivative term we use later in this work. The weak coupling means that we keep terms up to quadratic order in the coupling strength g_λ. In particular we have $\alpha(t) \sim \mathcal{O}\left(|g_\lambda|^2\right)$ and $z_t^*, \eta_t^* \sim \mathcal{O}(g_\lambda)$. The HOPS equations are obtained when the BCF is expanded into a sum of exponentials

$$\alpha(t) = \sum_\mu G_\mu e^{-W_\mu t},$$

and defining auxiliary states $|\psi_t^\mu(\mathbf{z}^*)\rangle = \int_0^t \mathrm{d}s\, G_\mu e^{-W_\mu(t-s)}\frac{\delta}{\delta z_s^*}|\psi_t(\mathbf{z}^*)\rangle$. The NMQSD equation now reads

$$\partial_t|\psi_t(\mathbf{z}^*)\rangle = -i(H_S + V(t))|\psi_t(\mathbf{z}^*\rangle + z_t^* L|\psi_t^*\rangle - L^\dagger\sum_\mu |\psi_t^\mu(\mathbf{z}^*)\rangle,$$

and the auxiliary states satisfy following equation of motion [55]

$$\partial_t|\psi_t^\mu(\mathbf{z}^*)\rangle = (-iH_S - iV(t) + z_t^* L - W_\mu)|\psi_t^\mu(\mathbf{z}^*)\rangle + G_\mu L|\psi_t(\mathbf{z}^*)\rangle - L^\dagger\sum_{\mu'}|\psi_t^{\mu\mu'}(\mathbf{z}^*)\rangle.$$

We truncate hierarchy to first order, which means that we neglect the last term. We also neglect the term $V(t)$ and z_t^* as they are proportional to g_λ. With these approximations we find

$$|\psi_t^\mu(\mathbf{z}^*)\rangle = \int_0^t \mathrm{d}s\, G_\mu \mathrm{e}^{-\mathrm{i}H_S(t-s) - W_\mu(t-s)} L|\psi_s(\mathbf{z}^*)\rangle.$$

As G_μ are already proportional to $|g_\lambda|^2$ we can replace $|\psi_s(\mathbf{z}^*)\rangle \approx e^{iH_S(t-s)}|\psi_t(\mathbf{z}^*)\rangle$ under the integral sign, which we obtained by integrating the NMQSD equation from backwards in time from t to s and keeping only the zeroth order terms. By considering the sum over all of the terms in the exponential expansion we obtain the weak coupling approximation

$$\int_0^t \mathrm{d}s\, \alpha(t-s)\frac{\delta}{\delta z_s^*}|\psi_t(\mathbf{z}^*)\rangle \approx \int_0^t \mathrm{d}s\, \alpha(t-s)e^{-iH_S(t-s)}Le^{iH_S(t-s)}|\psi_t(\mathbf{z}^*)\rangle. \quad (17)$$

We stress that these approximations lead to closed NMQSD equations of motion and correspond to a weak system bath coupling approximation [56]. Further refinements are possible in terms of HOPS, but we could explain the experimental data in this work using the weak coupling approximation only.

3.2 Susceptibility using NMQSD

Using the NMQSD we can compute the susceptibility of the system evolving pure states only. In case the coupling operator is Hermitian we need to evolve only one pure state, otherwise we need to average over the thermal noise [41]. In the case that we have multiple transition dipole moments we need to extend the NMQSD to many systems which all couple to their individual environments. This simply means that each subsystem has their own coupling operator L_m, noise term $z_{t,m}^*$, and bath correlation function $\alpha_m(t)$. We assume that the Hamiltonian is such that the global ground state is a product from the system ground state and the vacuum of the bath $|\Psi_G\rangle = |g_1, 0\rangle|g_2, 0\rangle \dots |g_N, 0\rangle$, where we consider N systems and $|0\rangle$ is the vacuum state of the environment of the respective open system. In the NMQSD approach the dipole correlation function $M(t)$ can be computed from the time-evolution [39]–[41]

$$M(t) = \mu_{tot}^2\langle\psi_0|\psi_t(\mathbf{z}^* = 0)\rangle, \quad (18)$$

where $|\psi_0\rangle$ is the initial state for the NMQSD evolution and $|\psi_t(\mathbf{z}^* = 0)\rangle$ is the solution to the NMQSD equation where the driving noise is set to zero, i.e. $z_t^* = 0$. The initial condition for the evolution is chosen as

$$|\psi_0\rangle = \frac{1}{\mu_{tot}}\sum_m e^{ik_z z_m}\mu_m|g\rangle, \quad \mu_{tot} = \sqrt{\sum_m |\mu_m|^2}. \quad (19)$$

If the coupling operator is Hermitian, we can replace the stochastic potential with the finite temperature bath correlation function

$$\alpha(t) = \int_0^\infty \mathrm{d}\omega\, J(\omega)\left(\coth\left(\frac{\beta\omega}{2}\right)\cos(\omega t) - i\,\sin(\omega t)\right). \quad (20)$$

Otherwise we need to average over different realizations of the thermal noise [39].

4 Molecular thin film

4.1 Description

The exciton of the TDAF is determined from experimentally measured absorption of a 60-nm-thick film of TDAF on a quartz substrate. The absorption is defined as $A = 1 - T - R$, where T and R are the fractions of the transmitted and reflected light, respectively. To accomplish the measurement of the reflected and transmitted light from the film without increasing the optical path length, the sample was excited at a 15° angle. We will model this process by computing the refractive index from a microscopic model and then the reflected and transmitted light using TMM [57].

4.2 Model

The dynamics of the molecule is governed by the Holstein model [26]

$$H_H = (\varepsilon_S + \zeta)\sigma_+\sigma_- + \sum_\lambda \omega_\lambda b_\lambda^\dagger b_\lambda + \sigma_+\sigma_-\sum_\lambda g_\lambda\left(b_\lambda + b_\lambda^\dagger\right). \quad (21)$$

We denote by $K = \sigma_+\sigma_-$ from now on. The system Hamiltonian and the coupling operator are in this case

$$H_S = (\varepsilon_S + \zeta)K, \quad L = K = K^\dagger, \quad (22)$$

where ζ is a disorder parameter. The coupling operator is Hermitian. The NMQSD equation in this case is

$$\frac{\mathrm{d}}{\mathrm{d}t}|\psi_t\rangle = \left(-iH_S + z_t^*K + \xi_t^*\sigma_- - \frac{\gamma}{2}K\right)|\psi_t\rangle - K\int_0^t \mathrm{d}s\, \alpha(t-s)\frac{\delta}{\delta z_s^*}|\psi_t\rangle, \quad (23)$$

where $\alpha(t-s)$ is the thermal BCF. We model the radiative damping by and additional white noise process ξ_t^* with correlation $\mathcal{M}\left[\xi_t\xi_s^*\right] = \gamma\delta(t-s)$. This model is not anymore solvable in closed form. If we neglected the radiative damping term, the model would admit an analytical solution [27].

For computing the susceptibility we can set both noise terms to zero. The spectral density is taken to be super-Ohmic with exponential cut-off [23]

$$J(\omega) = a\frac{\omega^u}{\xi^{u-1}}\mathrm{e}^{-\omega/\xi}, \quad u = 3, \tag{24}$$

where a is parameter additionally controlling the coupling strength. In the limit that the radiative damping is small compared to other parameters of the system the model admits a solution

$$|\psi_t\rangle \approx \exp\big(\big[-i(\varepsilon_s + \zeta - i\gamma/2)t - g(t)\big]K\big)|\psi_0\rangle, \tag{25}$$

where $g(t) = \int_{-\infty}^{t} \mathrm{d}s \int_{-\infty}^{s} \mathrm{d}u\, \alpha(u)$. We set the integration limits in this way to remove boundary terms and the reorganization energy term, which we absorb to the singlet energy. We do not highlight explicitly in the notation that the noises $\xi_t^* = z_t^* = 0$ anymore. The disorder ζ is distributed according to a Gaussian distribution with zero mean and standard deviation σ. As can be seen, the analytical solution is obtained by using Eq. (17). It turns out that this ansatz is exact for the Holstein model and also a good approximation for our model in the parameter regime relevant for this work.

4.3 Susceptibility

The dipole operator for this system is

$$\mu = \mu(\sigma_+ + \sigma_-), \tag{26}$$

with the abuse of notation we use the same symbol for the transition dipole operator and the transition dipole moment. Now the initial state given by (19) is the excited state $|e\rangle$ of the molecule. Inserting this and computing the average over the disorder gives the following expression for the dipole correlation function

$$M(t) = \exp\Big(-i(\varepsilon_s - i\gamma/2)t - \frac{1}{2}\sigma^2 t^2 - g(t)\Big) \tag{27}$$

In the case that $g(t) = 0$ this corresponds to the Voigt lineshape. The susceptibility is obtained by taking the Laplace transform from the dipole correlation function (27) and the refractive index can be readily computed.

4.4 Thin film absorption

The first singlet excited state is of the system is at $\varepsilon_S \approx 3.6$ eV as can be seen from the experimental trace in Figure 2. The radiative lifetime of the TDAF thin film is reported to be 133 ps ($\sim 10^{-5}$ eV) [58]. When fitting the model to the data we ensure that the standard deviation of the disorder parameter is larger than the radiative life time so that

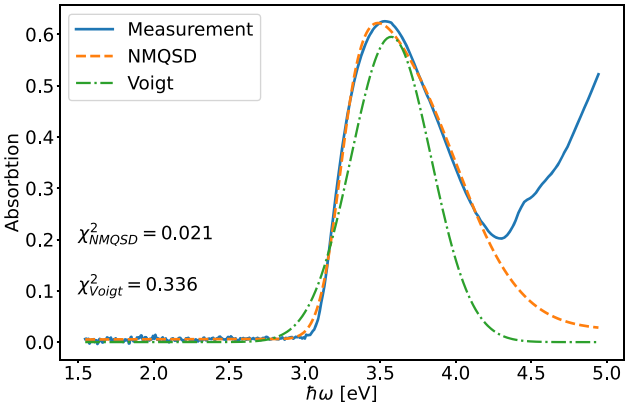

Figure 2: Absorption of a 60 nm thick thin film of TDAF molecules. The exciton energy is approximately 3.6 eV. Our model (NMQSD) fits well to the measured data, whereas a blind fit with a Voigt lineshape performs weaker in line with reported χ^2 values for each fit. The errorbars in the fit are smaller than the linewidth.

the solution (25) remains valid. For the above mentioned parameter values the thermal contributions to the dipole correlation function are insignificant and we use the zero temperature BCF when fitting the model to the experimental data.

The parameter values found in the fitting process are $\varepsilon_s = 3.6$ eV, $\sigma = 0.14$ eV, and $\xi = 0.09$. We kept the coupling strength parameter at a fixed value $a = 1$ and $\gamma = 5 \times 10^{-5}$ eV and included a background refractive index $n_{bg} = \sqrt{1.5 + 0.015i}$ to model the residual absorption at small energies. The reorganization energy for the fitted parameters is $\lambda_s \approx 0.19$ eV which is in agreement with the values reported in the DFT calculations [21]. The reorganization energy is absorbed in ε_s. The measured data, the fit using our model, and a blind fit to a Voigt lineshape are shown in Figure 2. The χ^2_{NMQSD} is significantly smaller than the χ^2_{Voigt}. We obtain the Voigt lineshape by neglecting the molecular vibrations contained in the term $g(t)$ in Eq. (27). This term is responsible for asymmetric broadening of the lineshape on higher energies.

4.5 Summary

We model the thin film of TDAF molecules as two level systems which each are coupled to their respective molecular vibrations and are probed by a weak classical electromagnetic field. We assume that there is no spatial disorder but the energies of the excitons are distributed according to Gaussian distribution with mean ε_s and variance σ. The macroscopic polarization is then obtained by multiplying the induced dipole moment with the number of molecules

in the sample. The inclusion of the disorder is motivated by the likeness of the experimental absorption lineshape to a Voigt profile and the fact that we found that thermal effects in our model were negligible in this parameter regime. The asymmetry in the absorption lineshape is explained by the coupling to the vibrational bath with spectral density given in Eq. (24). We find the parameter values by fitting the model to the experimentally measured absorption using TMM. The fitted parameters are the excitonic energy (ε_s), energy disorder (σ), coupling strength a, and the cut-off ξ. We keep the radiative lifetime of the exciton and the background refractive index constant during the fit. The fit of our model is very good and the obtained parameter values are in agreement with what is obtained from DFT calculations [21]. The quality of the fit justifies the use of approximate Eq. (25), which excludes for example possible direct interactions and cooperative effects between the molecules themselves.

5 Microcavity polariton reflectivity

5.1 System

The system is a 80 nm TDAF film in a cavity formed by two aluminium mirrors with thicknesses 25 nm and 100 nm. The reflectivity of this system can be measured experimentally as a function of the angle and energy of the incoming light. We again compute the refractive index from a microscopic model and then compare the reflectivity calculated using TMM with the experimental data.

5.2 Model

We follow [22], [59] in the construction of the model. The system consists of N molecules in a planar microcavity. The Hamiltonian for the molecules is

$$H_M = \sum_{m=1}^{N} \varepsilon_S K_m. \tag{28}$$

Photons in the cavity have the energy

$$\omega(\mathbf{k}) = \frac{c}{n_r}\sqrt{k_x^2 + k_z^2}, \tag{29}$$

where c is the speed of light in the vacuum and n_r is the refractive index of the propagation medium. $\mathbf{k}$ is the wave vector of the light which is assumed to be in the x–z plane. Mirrors at $x = \pm\frac{L}{2}$ confine the light in the x-direction so that the wavevector $k_x = m\pi/L$, where $m \in \mathbb{N}$. The cavity frequency at zero incidence is $\omega_0 = m\pi c/(n_r L)$. We restrict ourselves to $m = 1$ case, so that the cavity dispersion relation is

$$\omega(k_z) = \frac{c}{n_r}\sqrt{(\pi/L)^2 + k_z^2}. \tag{30}$$

Each mode has two orthogonal transverse polarizations $\mathbf{u}_1$ and $\mathbf{u}_2 = \frac{\mathbf{k}\times\mathbf{u}_1}{|\mathbf{k}|}$. The Hamiltonian for the cavity modes is then

$$H_C = \sum_{k_z} \omega(k_z) a_{k_z}^\dagger a_{k_z}, \tag{31}$$

where a_{k_z} is the annihilation operator for the cavity mode with the wave vector z-component k_z. The cavity modes couple to the transition dipole moment $\boldsymbol{\mu}_j$ with coupling strengths

$$g_m(k_z) = -\boldsymbol{\mu}_m \cdot \mathbf{u}\sqrt{\frac{\omega(k_z)}{2\varepsilon_0 V}}, \tag{32}$$

where $\mathbf{u}$ indicates the direction of the electric field of the confined mode, ε_0 is the vacuum permittivity, and V the cavity mode volume. We assume that the polarization of the cavity modes $\mathbf{u}$, the dipole moments $\boldsymbol{\mu}_j$, and the polarization of any incoming light are all aligned in the y-direction, thus we consider a situation described by Eq. (2). The coupling between the molecules and the cavity modes is given by the Tavis–Cummings interaction

$$H_{MC} = \sum_{m=1}^{N}\sum_{k_z} g_m(k_z)\left(\sigma_m^+ a_{k_z} e^{ik_z z_m} + h.c.\right), \tag{33}$$

where $e^{\pm ik_z z_j}$ describes the phase of the electric field of the cavity mode at the position z_j of the molecule j.

The coupling of each molecule to local vibrational modes is the same as in Section 4

$$H_{ME} = \sum_{m=1}^{N}\sum_{\lambda} g_\lambda K_m\left(b_{\lambda,m} + b_{\lambda,m}^\dagger\right), \tag{34}$$

where we assume that each molecule couples to its own bath of vibrational modes. The total Hamiltonian for the system is then

$$H_{HTC} = H_M + H_C + H_{MC} + H_{ME} + H_E, \tag{35}$$

where H_E is the free Hamiltonian for the vibrational modes

$$H_E = \sum_{m=1}^{N}\sum_{\lambda} \omega_\lambda b_{\lambda,m}^\dagger b_{\lambda,m}. \tag{36}$$

In addition, the cavity modes are damped with a rate that does not depend on k_z and we denote it by κ. The cavity damping is described in terms of additional zero mean white noise processes w_{t,k_z} with correlations

$$\mathcal{M}\left[w_{t,k_z} w_{s,k_z'}^*\right] = \kappa\delta_{k_z,k_z'}\delta(t-s), \quad \mathcal{M}\left[w_{t,k_z} w_{s,k_z'}\right] = 0. \tag{37}$$

Similarly, the excitons are damped with the rate γ, which is described by white noise processes $\xi_{t,j}$. The evolution of the system is given by the NMQSD equation which is trivially extended from the ones given earlier in the paper. Namely, we read off the terms of the NMQSD equation from the HTC Hamiltonian (Eq. (35)) and add independent excitonic and cavity dampings described by the white noise terms (Eq. (37)). Differently to the previous case, the thermal effects are significant and we use the non-zero temperature bath correlation function (Eq. (20)) in the subsequent calculations.

5.3 Susceptibility

We write the transition dipole moments for the molecules similarly as in Eq. (26) for each individual molecule. The dipole correlation function of this system can be calculated using (18). In this case the initial state (19)

$$|\psi_0\rangle = \frac{1}{\mu_{tot}} \sum_{m=1}^{N+1} e^{ik_z z_m} \mu_m |g\rangle, \tag{38}$$

is used. We take into account the possibility of light being absorbed by the cavity mode by an additional dipole moment $\mu_{N+1}(k_z) = \mu_c a_{k_z} + \mu_c^* a_{k_z}^\dagger$ with $z_{N+1} = 0$ reflecting the fact that the cavity mode is delocalized in the whole cavity volume. We can then calculate the linear susceptibility of the system from equation (6) and the refractive index. Our expression allows for the possibility that the classical electromagnetic field probing the system couples directly to the molecules as it is transmitted through the mirrors as well as indirectly after being first absorbed by the cavity mode. This is different than what is considered for example in [38], [42], where only cavity absorption is considered, which corresponds to the $\mu_m = 0$ limit of our results. We use the refractive index to calculate the reflectivity of the cavity system by using TMM for incoming light with the angular frequency ω and z-component of the wave vector k_z. These are related to the angle θ of the incoming light by

$$\omega = \frac{c|\mathbf{k}|}{n_r} = \frac{ck_z}{n_r \sin(\theta_c)} = \frac{ck_z}{\sin(\theta)}, \tag{39}$$

where θ_c is the angle inside the cavity and we have used the Snell's law.

5.4 Reflectivity

We show the computed and measured reflectivity in Figure 3 as a density plot. The quantitative agreement is good at small angles. For larger angles the locations of the polariton modes are in good qualitative agreement. In Figure 4 we show the computed and measured reflectivity as a function of the energy for different angles. There the disagreement at larger angles is more prominently visible. In Figure 4 we also present the estimated errorbars. We can conclude that for angles up to approximately 30° the model and the experiment are within the estimated errorbars. We discuss the errors involved in Section 6. In the TMM calculations the front mirror and the TDAF film is replaced with a material that has the computed refractive index. We use the parameters found in the fitting process

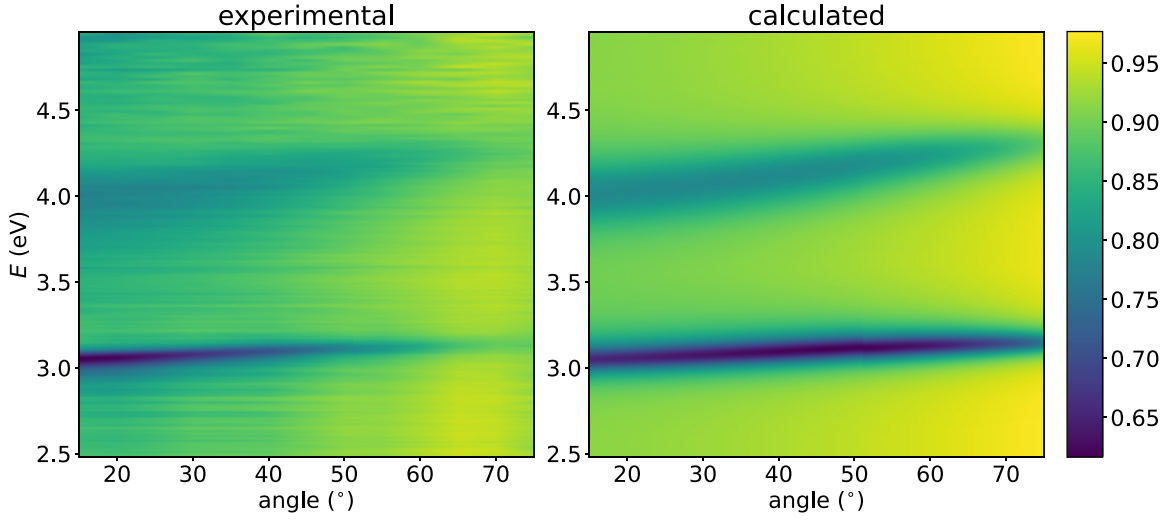

Figure 3: Experimental and calculated reflectivities for the cavity system. The qualitative agreement of the experiment and the theory is good. The reduced reflectivity of the upper polariton is due to the coupling to the vibrational modes. The agreement between our theory and the experiment is better at smaller angles.

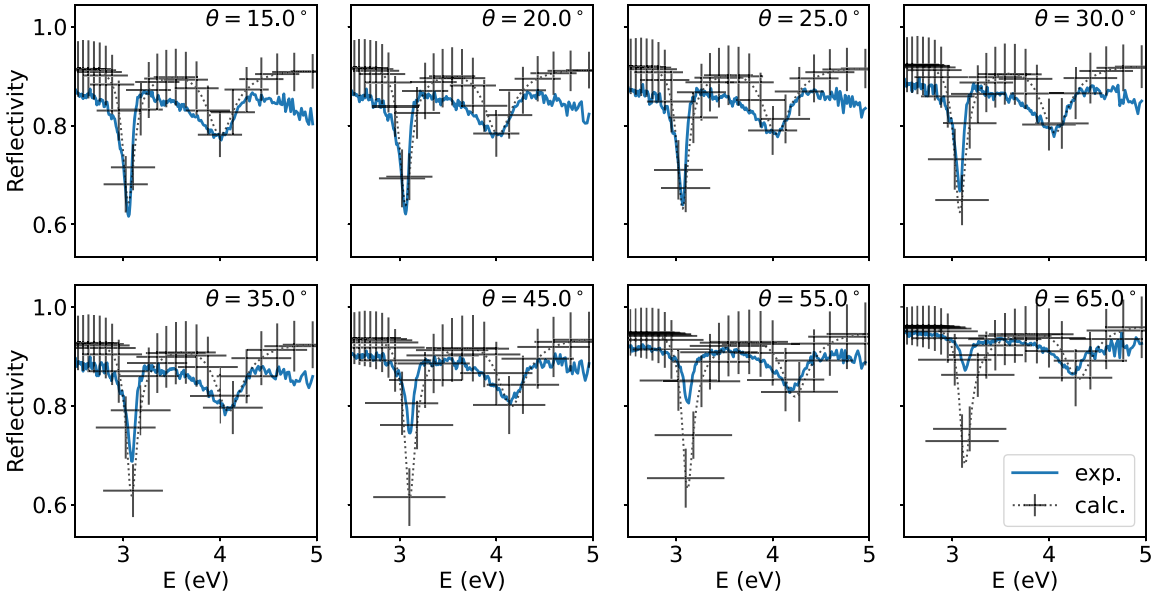

Figure 4: Error estimates for the polariton model. For small angles $\theta \leq 30°$ the location and amplitude of the computed and measured upper and lower polariton peaks are within the estimated error bars. For larger angles the model is in good qualitative agreement with the measured reflectivity and predicts the locations of the polariton peaks.

in Section 4. However, we set molecular disorder to zero and discuss this point in Section 6. To cover the full range of angles and energies used in the experiment, we use 21 cavity modes. Then the number of molecules is chosen to be high enough where additional increase does not change the reflectivity spectrum significantly. We choose $N = 84$. The cavity decay rate $\kappa = 0.21$ eV is estimated from experimental photoluminescence of the cavity system. We fitted the positions and depths of the reflectivity minima to the experimental data and got the values $n_r = 2.15$ for the refractive index that determines the cavity dispersion relation (30), $E(0) = 3.41$ eV for the energy of the cavity mode with $k_z = 0$, $\Omega = 0.91$ eV for the Rabi splitting, and $\mu_c = 3.5\mu_m$ for the magnitude of the cavity dipole moment.

With this model we can consider the classical field interacting with the system in three different ways. The first is that the light is absorbed by one of the cavity modes and there is no direct molecular absorption ($\mu_m = 0$). This makes the upper polariton absorb more and more as the angle increases because it becomes increasingly photonic. The second is that the light can only be absorbed by the molecules and $\mu_c = 0$. This results in both the upper and the lower polariton absorbing roughly the same amount. The third option is to include both cavity and molecular absorption which we found to match the experimental results the best. The vibrational coupling reduces the absorption of the upper polariton and this effect is greater at small angles where the polariton is mostly excitonic. Excluding this coupling would lead to pronounced absorption of the upper polariton in comparison to what is observed experimentally. Including quantum mechanical coupling to the vibrational modes and taking in account the possibility for both the molecular and the cavity mode absorption leads to an agreement between the experiment and our theory.

5.5 Summary

We extend the thin film model from Section 4 by including the dispersive cavity mode and spatial locations of the molecules. We have excluded the energy disorder of the excitons from the model. This is done because the effect of the energy disorder led to poor agreement with the model and the data. It may be that the approximations we do in our modeling do not correctly take into account the disorder and the coupling to the cavity modes. On the other hand, neglecting the effects of the exciton broadening are in line with the observations [60], [61], where the coupling to the cavity mode diminishes the exciton broadening effect. There, however, the cavities had higher Q factors than in our case. We estimate the error in our modeling by Monte Carlo sampling. We sample the computed reflectivity with randomly choosing the input parameters. We assume that all of the deviations are independent and distributed normally around the parameter values used in Figure 3. We consider the following deviations: The input energy has a standard

deviation $\sigma_E = 10^{-6}$ eV, the input angle $\sigma_\theta = 0.001°$, and the thickness of the system $\sigma_d = 10^{-9}$ m. We assume that the computed refractive index has energy dependent standard deviation $\sigma_n = 10^{-2}e^{-(\omega-\omega_0)/2}$ for the real and imaginary part, where ω_0 is the smallest energy used. The deviation is smaller for higher energies, which is necessary for obtaining meaningful errorbars around the polariton energies. The variations in the input parameters lead to two kinds of errors: the amplitude of the polariton peak and the location of the polariton peak may be wrong. The error bars in the location of the polaritons (x-axis) is taken to be the average variance of the estimated variances of the upper and lower polariton peak locations.

6 Conclusions and outlook

We have computed the susceptibility for organic microcavity polaritons from the Holstein–Tavis–Cummings model using non-Markovian quantum state diffusion. This approach is very efficient since we can compute susceptibility from evolving just a single state vector, so that density matrix computations are not needed. We have shown that our model can explain the absorptive properties of TDAF thin films and the reflectivity of the TDAF microcavity polaritons. In the thin film case the model explains the asymmetric shape of the absorption line very well. In the polariton case we do have good quantitative agreement around the polariton peaks at small angles ($\leq$30°) and good qualitative agreement at larger angles. We verify the modeling results with estimated error bars.

We have identified several open questions that will be the focus of our forthcoming investigations:

(i) We have seen that energetic disorder leads to a good fit in the thin film case but needs to be removed in the microcavity polariton case. Possible explanations used in the literature are the cavity filtering effect [60], [61] or motional narrowing [62], [63]. The former may not be the right explanation in this case since the cavities used in this work have such poor Q factors. The latter explanation fails as the spectroscopy we use conserves the planar wave vector of the cavity [45].

(ii) In this work we have relied on perturbative solutions to the NMQSD equation as they provided reasonable fits to the experiment. It will be interesting to investigate situations where such perturbative approaches fail. In such cases, there may be more complex intramolecular dynamics which may involve also the spin orbit coupling between the singlet and triplet states [23].

(iii) Lastly, we point out that state vector based approaches, such as NMQSD, open up a new way to study delocalization degree of the polaritons and polariton transport as it is possible to observe dynamically how the localization due to coupling to vibrational degrees of freedom and delocalization due to cavity coupling compete.

7 Methods

7.1 Fabrication

The samples were fabricated using thermal evaporation at a base pressure below 10^{-7} Torr (Angstrom Engineering physical vapor deposition system). We used 15 × 15 mm^2 quartz substrates that were cleaned by sonication for 10 min in soapy water (3 % Decon 90), acetone, and isopropanol, respectively, and dried with nitrogen. A 100-nm-thick aluminium was deposited on top of the substrate as the bottom mirror, followed by the deposition of 80 nm TDAF as the active layer, 1 nm of LiF, and a 25-nm-thick aluminium layer as a top polariton microcavity mirror.

7.2 Characterization

The TDAF absorption and polariton angle-resolved reflectivity were measured with a spectroscopic ellipsometer (J.A. Woollam VASE) in reflectivity and transmission configuration. To extract the absorption of TDAF film, we measured transmitted and reflected light at a 15° excitation angle, which represents the minimum angle our setup can measure reflectivity and adds only a 2 % increase in the optical path.

Acknowledgments: K.L. would like to thank Walter Strunz, Valentin Link, Kai Müller, and Christian Schäfer for fruitful discussions. The authors would like to thank the anonymous reviewers and Olli Siltanen for useful comments.

Research funding: This project has received funding from the European Research Council under the European Union's Horizon 2020 research and innovation programme (grant agreement No. [948260]) and from Business Finland project Turku-R2B-Bragg WOLED with decision number 1951/31/2021.

Author contributions: All authors have accepted responsibility for the entire content of this manuscript and approved its submission.

Conflict of interests: Authors state no conflicts of interest.

Informed consent: Informed consent was obtained from all individuals included in this study.

Ethical approval: The conducted research is not related to either human or animals use.

Data availability: The datasets generated during and/or analyzed during the current study are available from the corresponding author upon reasonable request.

References

[1] J. Keeling and S. Kéna-Cohen, "Bose-einstein condensation of exciton-polaritons in organic microcavities," *Annu. Rev. Phys. Chem.*, vol. 71, no. 1, p. 435, 2020.

[2] J. Tang, *et al*., "Room temperature exciton—polariton Bose—Einstein condensation in organic single-crystal microribbon cavities," *Nat. Commun.*, vol. 12, no. 1, p. 3265, 2021.

[3] A. J. Moilanen, K. S. Daskalakis, J. M. Taskinen, and P. Törmä, "Spatial and temporal coherence in strongly coupled plasmonic bose-einstein condensates," *Phys. Rev. Lett.*, vol. 127, no. 25, 2021, Art. no. 255301.

[4] G. W. Castellanos, M. Ramezani, S. Murai, and J. Gómez Rivas, "Non-equilibrium bose—einstein condensation of exciton-polaritons in silicon metasurfaces," *Adv. Opt. Mater.*, vol. 11, no. 7, 2023, Art. no. 2202305.

[5] A. Frisk Kockum, A. Miranowicz, S. De Liberato, S. Savasta, and F. Nori, "Ultrastrong coupling between light and matter," *Nat. Rev. Phys.*, vol. 1, no. 1, p. 19, 2019.

[6] A. V. Zasedatelev, *et al*., "Single-photon nonlinearity at room temperature," *Nature*, vol. 597, no. 7877, p. 493, 2021.

[7] D. Sanvitto and S. Kéna-Cohen, "The road towards polaritonic devices," *Nat. Mater.*, vol. 15, no. 10, p. 1061, 2016.

[8] M. Hertzog, M. Wang, J. Mony, and K. Börjesson, *Strong Light-Matter Interactions: A New Direction within Chemistry*, London, Royal Society of Chemistry, 2019.

[9] J. Y. Yuen-Zhou, L. A. Martínez-Martínez, J. B. Pérez-Sánchez, and K. Schwennicke, "Polariton chemistry: controlling organic photophysical processes with strong light-matter coupling," in *Physical Chemistry of Semiconductor Materials and Interfaces IX, August*, D. Congreve, C. Nielsen, and A. J. Musser, Eds., Bellingham, Washington, USA, SPIE, 2020, p. 23.

[10] (a) C. Ciuti and I. Carusotto, "Input-output theory of cavities in the ultrastrong coupling regime: the case of time-independent cavity parameters," *Phys. Rev. A*, vol. 74, no. 3, p. 033811, 2006. (b) F. J. Garcia-Vidal and T. W. Ebbesen, "Manipulating matter by strong coupling to vacuum fields," *Science*, vol. 373, no. 6551, p. eabd0336, 2021.

[11] R. Bhuyan, *et al*., "The rise and current status of polaritonic photochemistry and photophysics," *Chem. Rev.*, vol. 123, no. 18, pp.10877—10919, 2023.

[12] P. Törmä and W. L. Barnes, "Strong coupling between surface plasmon polaritons and emitters: a review," *Rep. Prog. Phys.*, vol. 78, no. 1, 2015, Art. no. 013901.

[13] E. Hulkko, S. Pikker, V. Tiainen, R. H. Tichauer, G. Groenhof, and J. J. Toppari, "Effect of molecular Stokes shift on polariton dynamics," *J. Chem. Phys.*, vol. 154, no. 15, 2021, Art. no. 154303.

[14] K. Stranius, M. Hertzog, and K. Börjesson, "Selective manipulation of electronically excited states through strong light—matter interactions," *Nat. Commun.*, vol. 9, no. 1, p. 2273, 2018.

[15] L. A. Martínez-Martínez, M. Du, R. F. Ribeiro, S. Kéna-Cohen, and J. Yuen-Zhou, "Polariton-assisted singlet fission in acene aggregates," *J. Phys. Chem. Lett.*, vol. 9, no. 8, p. 1951, 2018.

[16] A. M. Berghuis, *et al*., "Enhanced delayed fluorescence in tetracene crystals by strong light-matter coupling," *Adv. Funct. Mater.*, vol. 29, no. 36, 2019, Art. no. 1901317.

[17] E. Eizner, L. A. Martínez-Martínez, J. Yuen-Zhou, and S. Kéna-Cohen, "Inverting singlet and triplet excited states using strong light-matter coupling," *Sci. Adv.*, vol. 5, 2019, no. 12, Art. no. eaax4482.

[18] D. Polak, *et al*., "Manipulating molecules with strong coupling: harvesting triplet excitons in organic exciton microcavities," *Chem. Sci.*, vol. 11, no. 2, p. 343, 2020.

[19] Y. Yu, S. Mallick, M. Wang, and K. Börjesson, "Barrier-free reverse-intersystem crossing in organic molecules by strong light-matter coupling," *Nat. Commun.*, vol. 12, no. 1, p. 3255, 2021.

[20] A. Mukherjee, J. Feist, and K. Börjesson, "Quantitative investigation of the rate of intersystem crossing in the strong exciton—photon coupling regime," *J. Am. Chem. Soc.*, vol. 145, no. 9, p. 5155, 2023.

[21] A. G. Abdelmagid, *et al*., "Identifying the origin of delayed electroluminescence in a polariton organic light-emitting diode," *Nanophotonics*, 2024, https://doi.org/10.1515/nanoph-2023-0587 .

[22] R. H. Tichauer, J. Feist, and G. Groenhof, "Multi-scale dynamics simulations of molecular polaritons: the effect of multiple cavity modes on polariton relaxation," *J. Chem. Phys.*, vol. 154, no. 10, 2021, Art. no. 104112.

[23] L. A. Martínez-Martínez, E. Eizner, S. Kéna-Cohen, and J. Yuen-Zhou, "Triplet harvesting in the polaritonic regime: a variational polaron approach," *J. Chem. Phys.*, vol. 151, no. 5, p. 054106, 2019.

[24] M. Sánchez-Barquilla, F. J. García-Vidal, A. I. Fernández-Domínguez, and J. Feist, "Few-mode field quantization for multiple emitters," *Nanophotonics*, vol. 11, no. 19, p. 4363, 2022.

[25] K. Miwa, S. Sakamoto, and A. Ishizaki, "Control and enhancement of single-molecule electroluminescence through strong light—matter coupling," *Nano Lett.*, vol. 23, no. 8, p. 3231, 2023.

[26] T. Holstein, "Studies of polaron motion: Part i. the molecular-crystal model," *Ann. Phys.*, vol. 8, no. 3, p. 325, 1959.

[27] B. Krummheuer, V. M. Axt, and T. Kuhn, "Theory of pure dephasing and the resulting absorption line shape in semiconductor quantum dots," *Phys. Rev. B*, vol. 65, no. 19, 2002, Art. no. 195313.

[28] V. M. Agranovich, *Excitations in Organic Solids*, vol. 142, Oxford, England, OUP Oxford, 2009.

[29] V. M. Agranovich, M. Litinskaia, and D. G. Lidzey, "Cavity polaritons in microcavities containing disordered organic semiconductors," *Phys. Rev. B*, vol. 67, no. 8, 2003, Art. no. 085311.

[30] C. W. Gardiner and M. J. Collett, "Input and output in damped quantum systems: quantum stochastic differential equations and the master equation," *Phys. Rev. A*, vol. 31, no. 6, p. 3761, 1985.

[31] C. Ciuti and I. Carusotto, "Input-output theory of cavities in the ultrastrong coupling regime: the case of time-independent cavity parameters," *Phys. Rev. A*, vol. 74, no. 3, 2006, Art. no. 033811.

[32] N. Makri, "The linear response approximation and its lowest order corrections: an influence functional approach," *J. Phys. Chem. B*, vol. 103, no. 15, p. 2823, 1999.

[33] J. Ma and J. Cao, "Förster resonance energy transfer, absorption and emission spectra in multichromophoric systems. I. Full cumulant expansions and system-bath entanglement," *J. Chem. Phys.*, vol. 142, 2015, no. 9, Art. no. 094106.

[34] J. Ma, J. Moix, and J. Cao, "Förster resonance energy transfer, absorption and emission spectra in multichromophoric systems. II. Hybrid cumulant expansion," *J. Chem. Phys.*, vol. 142, no. 9, 2015, Art. no. 094107.

[35] J. M. Moix, J. Ma, and J. Cao, "Förster resonance energy transfer, absorption and emission spectra in multichromophoric systems.

III. Exact stochastic path integral evaluation," *J. Chem. Phys.*, vol. 142, no. 9, 2015, Art. no. 094108.
[36] G. Engelhardt and J. Cao, "Polariton localization and dispersion properties of disordered quantum emitters in multimode microcavities," *Phys. Rev. Lett.*, vol. 130, no. 21, 2023, Art. no. 213602.
[37] J. B. Pérez-Sánchez, A. Koner, N. P. Stern, and J. Yuen-Zhou, "Simulating molecular polaritons in the collective regime using few-molecule models," *Proc. Natl. Acad. Sci. U. S. A.*, vol. 120, no. 15, 2023, Art. no. e2219223120.
[38] J. Yuen-Zhou and A. Koner, *Linear response of Molecular Polaritons*, 2023, arXiv:2310.15424 [quant-ph].
[39] J. Roden, A. Eisfeld, W. Wolff, and W. T. Strunz, "Influence of complex exciton-phonon coupling on optical absorption and energy transfer of quantum aggregates," *Phys. Rev. Lett.*, vol. 103, no. 5, 2009, Art. no. 058301.
[40] J. Roden, W. T. Strunz, and A. Eisfeld, "Non-Markovian Quantum State Diffusion for absorption spectra of molecular aggregates," *J. Chem. Phys.*, vol. 134, no. 3, 2011, Art. no. 034902.
[41] G. Ritschel, D. Suess, S. Möbius, W. T. Strunz, and A. Eisfeld, "Non-Markovian Quantum State Diffusion for temperature-dependent linear spectra of light harvesting aggregates," *J. Chem. Phys.*, vol. 142, no. 3, 2015, Art. no. 034115.
[42] J. A. Ćwik, P. Kirton, S. De Liberato, and J. Keeling, "Excitonic spectral features in strongly coupled organic polaritons," *Phys. Rev. A*, vol. 93, no. 3, 2016, Art. no. 033840.
[43] K. S. Daskalakis, A. I. Väkeväinen, J.-P. Martikainen, T. K. Hakala, and P. Törmä, "Ultrafast pulse generation in an organic nanoparticle-array laser," *Nano Lett.*, vol. 18, no. 4, p. 2658, 2018.
[44] E. Palo, *et al*., "Developing solution-processed distributed bragg reflectors for microcavity polariton applications," *J. Phys. Chem. C*, vol. 127, no. 29, 2023, Art. no. 14255.
[45] A. Kavokin, J. Baumberg, G. Malpuech, and F. Laussy, *Microcavities*, *Series on Semiconductor Science and Technology*, Oxford, England, OUP Oxford, 2007.
[46] G. Panzarini, *et al*., "Cavity-polariton dispersion and polarization splitting in single and coupled semiconductor microcavities," *Phys. Solid State*, vol. 41, no. 8, p. 1223, 1999.
[47] V. May and O. Kühn, *Charge and Energy Transfer Dynamics in Molecular Systems*, Hoboken, New Jersey, U.S., Wiley, 2011.
[48] H. Haug and S. Koch, *Quantum Theory of the Optical and Electronic Properties of Semiconductors, G - Reference,Information and Interdisciplinary Subjects Series*, Singapore, World Scientific, 2004.
[49] C. Klingshirn, *Semiconductor Optics*, Springer Study Edition, Berlin, Germany, Springer Berlin Heidelberg, 1997.
[50] L. Diósi, N. Gisin, and W. T. Strunz, "Non-markovian quantum state diffusion," *Phys. Rev. A*, vol. 58, no. 3, p. 1699, 1998.
[51] R. Hartmann and W. T. Strunz, "Exact open quantum system dynamics using the hierarchy of pure states (hops)," *J. Chem. Theory Comput.*, vol. 13, no. 12, p. 5834, 2017.
[52] N. Megier, W. T. Strunz, C. Viviescas, and K. Luoma, "Parametrization and optimization of Gaussian non-markovian unravelings for open quantum dynamics," *Phys. Rev. Lett.*, vol. 120, no. 15, 2018, Art. no. 150402.
[53] V. Link, K. Luoma, and W. T. Strunz, "Non-markovian quantum state diffusion for spin environments," *New J. Phys.*, vol. 25, no. 9, 2023, Art. no. 093006.
[54] P. Goetsch, R. Graham, and F. Haake, "Microscopic foundation of a finite-temperature stochastic Schrödinger equation," *Quantum Semiclassical Opt. J. Eur. Opt. Soc. Part B*, vol. 8, no. 1, p. 157, 1996.
[55] D. Suess, A. Eisfeld, and W. T. Strunz, "Hierarchy of stochastic pure states for open quantum system dynamics," *Phys. Rev. Lett.*, vol. 113, no. 15, 2014, Art. no. 150403.
[56] T. Yu, L. Diósi, N. Gisin, and W. T. Strunz, "Non-markovian quantum-state diffusion: perturbation approach," *Phys. Rev. A*, vol. 60, no. 1, p. 91, 1999.
[57] S. J. Byrnes, *Multilayer Optical Calculations*, 2020, arXiv:1603.02720 [physics.comp-ph].
[58] S. Toffanin, *et al*., "Molecular host-guest energy-transfer system with an ultralow amplified spontaneous emission threshold employing an ambipolar semiconducting host matrix," *J. Phys. Chem. B*, vol. 114, no. 1, p. 120, 2010.
[59] P. Michetti and G. C. La Rocca, "Polariton states in disordered organic microcavities," *Phys. Rev. B*, vol. 71, no. 11, 2005, Art. no. 115320.
[60] M. Wurdack, *et al*., "Motional narrowing, ballistic transport, and trapping of room-temperature exciton polaritons in an atomically-thin semiconductor," *Nat. Commun.*, vol. 12, no. 1, p. 5366, 2021.
[61] R. Pandya, *et al*., "Tuning the coherent propagation of organic exciton-polaritons through dark state delocalization," *Adv. Sci.*, vol. 9, no. 18, 2022, Art. no. 2105569.
[62] D. M. Whittaker, *et al*., "Motional narrowing in semiconductor microcavities," *Phys. Rev. Lett.*, vol. 77, no. 23, p. 4792, 1996.
[63] A. V. Kavokin, *et al*. "Motional narrowing of in homogeneously broadened excitons in a semiconductor microcavity: semiclassical treatment," *Phys. Rev. B*, vol. 57, no. 7, p. 3757, 1998.